REPORT NO.
UCB/SESM-82/04

STRUCTURAL ENGINEERING AND
STRUCTURAL MECHANICS

OPERATOR SPLIT METHODS IN THE NUMERICAL SOLUTION OF THE FINITE DEFORMATION ELASTOPLASTIC DYNAMIC PROBLEM

by

PETER M. PINSKY

MIGUEL ORTIZ

and

ROBERT L. TAYLOR

MAY 1982

DEPARTMENT OF CIVIL ENGINEERING
UNIVERSITY OF CALIFORNIA
BERKELEY, CALIFORNIA

OPERATOR SPLIT METHODS IN THE NUMERICAL SOLUTION OF THE FINITE DEFORMATION ELASTOPLASTIC DYNAMIC PROBLEM

Peter M. Pinsky, Miguel Ortiz and Robert L. Taylor

Division of Structural Engineering and Structural Mechanics
Department of Civil Engineering
University of California, Berkeley

ABSTRACT

The spatial formulation of the elastoplastic dynamic problem for finite deformations is considered. A thermodynamic argument leads to an additive decomposition of the spatial rate of deformation tensor and allows an operator split of the evolutionary equations of the problem into "elastic" and "plastic" parts. This operator split is taken as the basis for the definition of a global product algorithm. In the context of finite element discretization the product algorithm entails, for every time step, the solution of a nonlinear elastodynamic problem followed by the application of plastic algorithms that operate on the stresses and internal variables at the integration points and bring in the plastic constitutive equations. Suitable plastic algorithms are discussed for the cases of perfect and hardening plasticity and viscoplasticity. The proposed formalism does not depend on any notion of smoothness of the yield surface and is applicable to arbitrary convex elastic regions, with or without corners. The stability properties of the global product algorithm are shown to be identical to those of the algorithm used for the integration of the nonlinear elastodynamic problem. Numerical examples illustrate the accuracy of the method.

June 27, 1982

OPERATOR SPLIT METHODS IN THE NUMERICAL SOLUTION OF THE FINITE DEFORMATION ELASTOPLASTIC DYNAMIC PROBLEM

Peter M. Pinsky, Miguel Ortiz and Robert L. Taylor

Division of Structural Engineering and Structural Mechanics

Department of Civil Engineering

University of California, Berkeley

1. Introduction

A variety of techniques have been proposed for the numerical treatment of the finite deformation elastoplastic boundary value problem [4,7,13,19]. Those based on some notion of an elastoplastic modulus tensor, such as the tangent modulus tensor method, suffer from various shortcomings. For instance, the methods are ill-suited for dealing with corners in the yield surface. Furthermore, the consistency condition of plasticity which requires that the stress trajectory be confined to the elastic domain is difficult to enforce exactly. Frequently, projection techniques have been introduced to restore consistency. In addition, these methods require elaborate schemes for making the transition from the elastic into the plastic regimes that frequently involve discarding or truncating time steps.

The limitations associated with the above methods have motivated the search for alternative methods of solution. One such alternative method makes use of the concept of a "return mapping" algorithm and was originally proposed by Mendelson [32] for the case of infinitesimal deformations. This technique consists of solving for every time step an incremental linear elastic problem followed by the application of a return mapping algorithm to the stresses to restore consistency. Clearly, this procedure automatically guarantees the satisfaction of the consistency condition. Moreover, the method results in unconditional stability [33] and reasonable accuracy [29,30,31].

In order to be convergent, numerical solution schemes have to satisfy the requirements of consistency and numerical stability. A formal study of the consistency and numerical stability properties of the global solution schemes arising from the use of return mapping algorithms is missing in the literature. At best, the existing work has only considered partial aspects of the global numerical solution scheme such as the integration of the constitutive equations [29,30,31]. It is shown in this paper how the operator split formalism provides a suitable framework in which these issues can be adequately studied.

The operator split method, briefly discussed in Section 2, has recently been applied within the context of computational mechanics and shows considerable potential as a tool for the analysis of certain classes of linear and nonlinear problems [1,2]. For instance, this technique has been recently used in connection with the heat conduction problem [2] and the structural dynamics problem [1].

In Section 3 a spatial formulation of the elastoplastic dynamic problem for finite deformations is developed. Central to the applicability of the operator split method to the elastoplastic dynamic problem is the additive decomposition of the spatial rate of deformation tensor into "elastic" and "plastic" parts. A brief discussion presenting a thermodynamic basis for such a decomposition is also presented in Section 3.

In Section 4 an operator split of the field equations into "elastic" and "plastic" parts is introduced. Product formula techniques are then applied to this additive decomposition, resulting in a step-by-step integration procedure in which a nonlinear elastodynamic problem is first solved, followed by the application of algorithms that bring in the plastic part of the field equations. The nonlinear elastodynamic problem is solved by means of a Newton-Raphson procedure based on consistent linearization of a weak form of the boundary value problem for momentum balance. The elastic rate constitutive equations are numerically integrated using an unconditionally stable and incrementally objective algorithm.

For the rate-independent case, it is shown in Section 4 that the algorithms for the integration of the plastic part of the field equations are return mapping algorithms in which the stresses corresponding to the elastic solution are projected into the elastic region by means of general return mappings. For the viscoplastic case, the plastic algorithms are shown to represent a relaxation process of the stresses towards the elastic region. In this context, the consistency and numerical stability of the resulting global solution schemes is demonstrated. The numerical stability properties of the elastoplastic product algorithm are shown to be identical to those of the algorithm employed in the integration of the elastic part of the equations of motion. Also, the return mapping technique is extended to the dynamic, viscoplastic and hardening cases.

The proposed formalism does not depend on any notion of smoothness of the yield hypersurface and is applicable to arbitrary convex elastic regions with or without corners. Under appropriate conditions, it is shown that the viscoplastic solution approximates the rate independent one in the limit of small viscosities. Finally, the accuracy of the method is demonstrated by means of numerical examples.

2. General Product Algorithms Based on Operator Splits of Equations of Evolution

In the present section, a collection of results is presented regarding operator split methods and product formula algorithms for general nonlinear equations of evolution. These results illustrate the point that product formulas can be advantageously applied to any set of equations of evolution where the evolutionary operator has an additive decomposition (operator split) into several, hopefully simpler, component operators. The basic idea underlying product formulas is that of treating each one of the component operators independently. In a typical integration process, one applies an algorithm to the solution vector that is consistent with the first component operator, the result of which is then operated upon with an algorithm which is consistent with the second component operator, and so on.

Often in the numerical treatment of engineering problems one is led to consider equations of evolution of the following general form

$$\mathbf{A}\,\dot{\mathbf{x}} + \mathbf{B}(\mathbf{x}) = \mathbf{f}\ ; \qquad \mathbf{x}(0) = \mathbf{x}_o \tag{1}$$

a particular case of which is the unforced equation

$$\mathbf{A}\,\dot{\mathbf{x}} + \mathbf{B}(\mathbf{x}) = 0\ ; \qquad \mathbf{x}(0) = \mathbf{x}_o \tag{2}$$

In the above, $\mathbf{x}$ is an s-dimensional vector, $\mathbf{A}$ is a positive definite symmetric matrix and $\mathbf{B}$ is a nonlinear function from R^s into R^s.

It is useful for the subsequent discussion to endow R^s with the "energy" inner product $<\mathbf{x},\mathbf{y}> = \mathbf{x}^T\mathbf{A}\mathbf{y}$ for every $\mathbf{x},\mathbf{y} \in R^s$, having an associated norm $||\mathbf{x}||^2 = <\mathbf{x},\mathbf{x}>$.

In this context, an unconditionally stable algorithm for equation (2) is a one-parameter family of (nonlinear) functions $\mathbf{F}(h) : R^s \rightarrow R^s$, $h > 0$, satisfying

1) Consistency:

$$\lim_{h \rightarrow 0^+} \mathbf{A}\,\frac{\mathbf{F}(h)\mathbf{x} - \mathbf{x}}{h} = \mathbf{B}(\mathbf{x}) \quad \textit{for every}\ \ \mathbf{x} \in R^s \tag{3}$$

2) Unconditional stability:

$$||\mathbf{F}(h)\,\mathbf{x} - \mathbf{F}(h)\,\mathbf{y}|| \leqslant ||\mathbf{x} - \mathbf{y}|| \quad \textit{for every}\ \ \mathbf{x},\mathbf{y} \in R^s,\ \ h>0. \tag{4}$$

In the linear case, the mapping $\mathbf{F}(h)$ is linear in $\mathbf{x}$ and the stability condition (4) reduces to the simpler form $||\mathbf{F}(h)\,\mathbf{x}|| \leqslant ||\mathbf{x}||$ for every $\mathbf{x} \in R^s$. This in turn implies that the norm $||\mathbf{F}(h)|| \leqslant 1$. Recalling the inequality $\rho(\mathbf{F}(h)) \leqslant ||\mathbf{F}(h)||$, relating the spectral radius $\rho(\mathbf{F}(h)) \equiv \inf_n ||\mathbf{F}(h)^n||^{1/n}$ to the norm of $\mathbf{F}(h)$, it may be seen that the stability condition (4) is in general more stringent than the usual concept of stability that requires $\rho(\mathbf{F}(h)) \leqslant 1$. If $\mathbf{F}(h)$ is a stable algorithm for (2) in the sense of (3) and (4) then convergence is guaranteed under mild conditions on $\mathbf{B}$ [3].

In a variety of problems in mechanics the evolutionary operator $\mathbf{B}$ and the forcing term $\mathbf{f}$ admit an additive decomposition

$$\mathbf{B} = \sum_{i=1}^{N} \mathbf{B}_i \quad ; \quad \mathbf{f} = \sum_{i=1}^{N} \mathbf{f}_i . \tag{5}$$

We are concerned here with the problem of constructing a class of computationally efficient algorithms that exploit the additive form of $\mathbf{B}$ and $\mathbf{f}$.

Let $\mathbf{F}_i(h)$, $i = 1, 2, \cdots, N$ denote stable algorithms consistent with $\mathbf{A}$ and $\mathbf{B}$. The corresponding global product algorithm then takes the form

$$\mathbf{F}(h) = \mathbf{F}_N(h)\,\mathbf{F}_{N-1}(h) \cdots \mathbf{F}_1(h) \equiv \prod_{i=1}^{N} \mathbf{F}_i(h) \tag{6}$$

In other words, the algorithm $\mathbf{F}(h)$ amounts to applying the individual algorithms $\mathbf{F}_i(h)$ consecutively to the solution vector, taking the result from each one of these applications as the initial conditions for the next algorithm. The global algorithm is complete for a given time step when all the individual algorithms have been applied.

It is shown in [1] that if all the individual algorithms $\mathbf{F}_i(h)$ are consisistent with $\mathbf{A}$ and $\mathbf{B}$, in the sense of (3), then the global product algorithm $\mathbf{F}(h)$ defined by (6) is consistent with $\mathbf{A}$ and $\mathbf{B}$. It is further shown in [1] that if all the individual algorithms $\mathbf{F}_i(h)$ are unconditionally stable in the sense of (4), then the global product algorithm $\mathbf{F}(h)$ is also unconditionally stable. In other words the norm stability of the individual algorithms, in the sense of (4), is preserved by the product formula (6). It is interesting to note, on the other hand, that no general statements can be made about the stability of the product formula in the sense of the spectral ratio, given that, unlike the norm, this quantity is not well-behaved with respect to matrix multiplications. A general discussion of these and other related issues can be found in [1]. Some of these results have also been discussed in [2] for the particular case of linear equations of evolution and the trapezoidal rule.

In Section 4, global product algorithms will be employed in connection with an additive decomposition of the evolutionary operator governing the finite deformation elastoplastic dynamic problem.

3. Field Equations for Finite Deformation Elastoplasticity.

3.1. Preliminaries

In this section, definitions of tensors required for subsequent discussions are stated and connections among certain of these are established. For a complete account of the continuum basis underlying constitutive theory the interested reader is referred to [22,23].

A motion of a deformable body in the ambient space R^N, relative to a reference configuration B, is given by a time dependent mapping $\phi_t(\mathbf{X}) : B \rightarrow R^N$, $t > 0$. Here, $\mathbf{X}$ denotes a set of material coordinates defined on the reference configuration.

The material velocity of the motion ϕ_t is defined as a vector field $\mathbf{V}$ over the reference configuration, such that $\mathbf{V} = \frac{d}{dt}\phi_t$ The spatial velocity field $\mathbf{v}$ is defined by $\mathbf{v} = \mathbf{V} \circ \phi_t^{-1}$. Note that the spatial velocity field $\mathbf{v}(\mathbf{x},t)$ is dependent on a set of spatial coordinates denoted $\mathbf{x}$.

The deformation gradient is defined by $\mathbf{F} = \frac{\partial \phi}{\partial \mathbf{X}}$ with components, $F^a{}_A = \frac{\partial \phi^a}{\partial X^A}$. From $\mathbf{F}$ one can obtain the Jacobian of the motion $J = \det \mathbf{F}$ and the right Cauchy-Green deformation tensor $\mathbf{C}$ which is related to the deformation gradient by $\mathbf{C} = \mathbf{F}^T \cdot \mathbf{F}$.

The spatial velocity gradient tensor $\mathbf{l}$ is given by $\mathbf{l} = \nabla \mathbf{v}$, where ∇ denotes the gradient with respect to the spatial coordinates $\mathbf{x}$. The symmetric part of $\mathbf{l}$, $\mathbf{d} \equiv \nabla^S \mathbf{v}$ is the spatial rate of deformation tensor, and the skewsymmetric part $\boldsymbol{\omega} \equiv \nabla^A \mathbf{v}$ is the spin rate or vorticity tensor.

If γ is a tensor field defined on the deformed configuration $\phi_t(B)$, the pull back of γ through the motion ϕ_t defines a tensor field Γ on B denoted by $\Gamma = \phi_t^*(\gamma)$ For example, in the case of a second order contravariant tensor the pull back operation takes the form

$$\Gamma^{AB} = (F^{-1})^A{}_a \, (F^{-1})^B{}_b \, (\gamma^{ab} \circ \phi_t).$$

This definition may be readily generalized to spatial tensor fields of any order.

Likewise, if Γ is a material tensor field defined on B, the push forward of Γ through the motion ϕ_t defines a spatial tensor field γ on $\phi_t(B)$ denoted by $\gamma = \phi_{t*}(\Gamma)$. In this case, for the example used above, the push forward operation takes the form

$$\gamma^{ab} = F^a{}_A \, F^b{}_B \, (\Gamma^{AB} \circ \phi_t^{-1}).$$

A related concept associated with the push forward of material rates of material tensors is that of the Lie derivative of a spatial tensor with respect to the spatial velocity field. The Lie derivative entails pulling back the spatial tensor to the reference configuration, taking the material time derivative of the resulting material tensor and pushing forward the result into the current configuration. Formally, for a spatial tensor $\boldsymbol{\gamma}$,

$$L_{\mathbf{v}}(\boldsymbol{\gamma}) \equiv \boldsymbol{\phi}_{t*}\left[\frac{d}{dt}\boldsymbol{\phi}_t^{*}(\boldsymbol{\gamma})\right] \tag{7}$$

This notation allows for a compact expression of many relations in continuum mechanics. For example, the Cauchy stress tensor $\boldsymbol{\sigma}$ defined on the current configuration and the second Piola-Kirchhoff stress tensor $\mathbf{S}$ associated with the reference configuration are related by

$$\mathbf{S} = J\boldsymbol{\phi}_t^{*}(\boldsymbol{\sigma}) \quad or \quad \boldsymbol{\sigma} = \boldsymbol{\phi}_{t*}(J^{-1}\mathbf{S})$$

These relations, involving J, are called Piola transformations.

The forward Piola transformation of the material time derivative of S, denoted $\overset{\circ}{\boldsymbol{\sigma}}$, is

$$\overset{\circ}{\boldsymbol{\sigma}} = \boldsymbol{\phi}_{t*}(J^{-1}\dot{\mathbf{S}}), \tag{8}$$

the so-called Truesdell rate of Cauchy stress. For contravariant components (8) has the form

$$\overset{\circ}{\boldsymbol{\sigma}} = \dot{\boldsymbol{\sigma}} - \mathbf{l}\cdot\boldsymbol{\sigma} - \boldsymbol{\sigma}\cdot\mathbf{l}^T + \boldsymbol{\sigma}\, tr(\mathbf{d})$$

where $\dot{\boldsymbol{\sigma}}$ denotes the material time derivative of $\boldsymbol{\sigma}$ given by $\dot{\boldsymbol{\sigma}} = \dfrac{\partial\boldsymbol{\sigma}}{\partial t} + \nabla\boldsymbol{\sigma}\cdot\mathbf{v}$. Alternatively, in terms of the Lie derivative, (8) can be written

$$\overset{\circ}{\boldsymbol{\sigma}} = J^{-1}\boldsymbol{\phi}_{t*}\left[\frac{d}{dt}\boldsymbol{\phi}_t^{*}(J\boldsymbol{\sigma})\right] = J^{-1}L_{\mathbf{v}}(\boldsymbol{\tau}) \tag{9}$$

where $\boldsymbol{\tau} \equiv (J \circ \boldsymbol{\phi}_t^{-1})\,\boldsymbol{\sigma}$ is the Kirchhoff stress tensor. These relations will prove to be useful in subsequent sections where their relevance is discussed in detail.

It is noted that the Truesdell rate is objective [18,22]. The principle of objectivity requires that intrinsic physical properties of a body be independent of the body's location or orientation in space. This principle is embodied in constitutive theory by requiring that constitutive equations contain only objective tensor fields. Consequently, the Truesdell rate of Cauchy stress may be considered as a candidate for use in spatial rate constitutive equations.

Many other objective rates have been proposed within the context of constitutive theory. A frequent choice is the Jaumann, or co-rotational rate of Kirchhoff stress,

$$\overset{\nabla}{\tau} = \dot{\tau} - \omega \cdot \tau + \tau \cdot \omega$$

The significance of the Jaumann rate as it relates to constitutive theory and its connection with the Truesdell rate has been considered in [18,28]

The local form of linear momentum balance together with traction and kinematic boundary conditions can be expressed as

$$\begin{aligned} \rho \dot{\mathbf{v}} &= \nabla \cdot \boldsymbol{\sigma} + \rho \mathbf{b} \qquad \mathbf{x} \in \boldsymbol{\phi}_t(B) \\ \boldsymbol{\sigma} \cdot \mathbf{n} &= \bar{\mathbf{t}} \qquad \mathbf{x} \in \partial_\sigma \boldsymbol{\phi}_t(B) \\ \boldsymbol{\phi} &= \bar{\boldsymbol{\phi}} \qquad \mathbf{x} \in \partial_u \boldsymbol{\phi}_t(B) \end{aligned} \tag{10}$$

where ρ is the mass density in $\boldsymbol{\phi}_t(B)$, $\mathbf{b}$ is a spatial body force field, and $\bar{\mathbf{t}}$ and $\bar{\boldsymbol{\phi}}$ are the prescribed tractions and motion over the traction and kinematic boundaries $\partial_\sigma \boldsymbol{\phi}_t(B)$ and $\partial_u \boldsymbol{\phi}_t(B)$, respectively.

In order to have a complete set of equations suitable constitutive equations need to be specified. The form of these equations for a limited class of elastoplastic materials is the subject of the next section.

3.2. Rate Constitutive Equations for Finite Deformation Elastoplasticity

In analysis of finite deformation problems the use of constitutive equations in rate form is often required. In a spatial setting, these equations express a relationship between some objective rate of a spatial stress tensor, such as the Cauchy or Kirchhoff stress tensor, and the rate of deformation.

Rate constitutive relations can be alternatively formulated in a material or a spatial setting. The former case involves rates of material tensors which are always objective. In a spatial formulation, however, material rates of objective tensors are not objective and so-called objective stress rates, such as the Truesdell or Jaumann rates, must be introduced. This has the effect of introducing additional complexity in the development of integration algorithms for rate constitutive equations and has motivated recent research in the area [19,20,28].

The correct choice of spatial rate constitutive equations has been the subject of considerable conjecture [21,24,25,26,27], inasmuch as the principle of objectivity alone does not uniquely determine the choice of objective stress rate. It is noted, however, that the material and spatial formulations are equivalent expressions of the same physical principles and are therefore uniquely related to each other. This assertion rests on the fact that the mathematical formulation of the principles of mechanics has to be invariant with respect to the choice of reference configuration [22]. It has been shown in [28] that when this additional principle is invoked, indeterminacy in the choice of objective stress rate is removed.

The following discussion is concerned with the problem of deriving adequate spatial rate constitutive equations. The approach taken is based on a thermodynamic formulation of constitutive equations in a material setting, the spatial representation of which is then consistently derived.

The existence of a complementary free energy potential per unit mass of B, denoted $\chi(\mathbf{S}, \mathbf{Q})$, is assumed. Here, $\mathbf{S}$ is the second Piola-Kirchhoff stress tensor and $\mathbf{Q}$ denotes a set of internal variables defined on the reference configuration B. The justification for such an assumption is discussed in [9].

From the Clausius-Duhem inequality [9,10] it can be shown that the complementary free energy is a potential for the right Cauchy-Green deformation tensor $\mathbf{C}$, i.e.,

$$\mathbf{C} = 2\rho_o \frac{\partial \chi}{\partial \mathbf{S}} \tag{11}$$

where ρ_o denotes the reference mass density. A rate form of (11) is obtained by taking the material time derivative, resulting in

$$\dot{\mathbf{C}} = \mathbf{M} : \dot{\mathbf{S}} + \mathbf{N} \cdot \dot{\mathbf{Q}} \tag{12}$$

where $\mathbf{M}$ is the material elasticity tensor, defined by $\mathbf{M} = 2\rho_o \dfrac{\partial^2 \chi}{\partial \mathbf{S}^2}$ and $\mathbf{N}$ is an inelastic compliance tensor defined by $\mathbf{N} = 2\rho_o \dfrac{\partial^2 \chi}{\partial \mathbf{Q} \partial \mathbf{S}}$. Since material time derivatives of material tensors are objective, constitutive equation (12) is also objective.

A spatial form of constitutive eq. (12) can be obtained as follows. Noting that $\dot{\mathbf{C}} = 2\boldsymbol{\phi}_t^*(\mathbf{d})$ and eq. (8), the forward Piola transformation of eq. (12) reads

$$\mathbf{d} = \mathbf{m} : \overset{\circ}{\boldsymbol{\sigma}} + \mathbf{n} \cdot \overset{\circ}{\mathbf{q}} \tag{13}$$

where $\mathbf{m} = \frac{1}{2} J \boldsymbol{\phi}_{,*}(\mathbf{M})$ is the spatial elasticity tensor, $\mathbf{n} = \frac{1}{2} J \boldsymbol{\phi}_{,*}(\mathbf{N})$ is a spatial inelastic compliance tensor, $\mathbf{q} = \boldsymbol{\phi}_{,*}(J^{-1}\mathbf{Q})$ are the spatial internal variables and $\overset{\circ}{\mathbf{q}} = \boldsymbol{\phi}_{,*}(J^{-1}\dot{\mathbf{Q}})$ is the Truesdell rate of $\mathbf{q}$.

Equation (13) has the interpretation that the total deformation rate $\mathbf{d}$ has an additive decomposition into an "elastic" part $\mathbf{d}^e = \mathbf{m} : \overset{\circ}{\boldsymbol{\sigma}}$ and an "inelastic" or "plastic" part $\mathbf{d}^p = \mathbf{n} \cdot \overset{\circ}{\mathbf{q}}$, i.e.,

$$\mathbf{d} = \mathbf{d}^e + \mathbf{d}^p \tag{14}$$

This decomposition has been obtained independently of any kinematic considerations. Other theories of plasticity [11,12,14] have been based on different kinematic assumptions. By appropriate definitions of the kinematic variables these theories can be brought into correspondence with eq. (14). Eq. (14) has the alternative form

$$\overset{\circ}{\boldsymbol{\sigma}} = \mathbf{a} : (\mathbf{d} - \mathbf{d}^p) \tag{15}$$

where $\mathbf{a} = \mathbf{m}^{-1}$ is the spatial elastic modulus tensor. Further details regarding the above discussion can be found in [18].

In order to have a complete set of constitutive equations one has to supplement eq. (15) with some constitutive relations for $\mathbf{d}^p$ and $\mathbf{q}$. For the time being, it will suffice to assume that $\mathbf{d}^p$ can be expressed as a function of the stresses and the spatial internal variables $\mathbf{q}$, i.e.,

$$\mathbf{d}^p = \mathbf{T}(\boldsymbol{\sigma}, \mathbf{q}) \tag{16}$$

The internal variables $\mathbf{q}$ may for example represent the yield stress for an isotropic hardening model or the translation of the elastic domain for a kinematic hardening model. Eq. (16) is general enough to accommodate perfect and hardening viscoplasticity. Specific examples of such constitutive relations that are widely used in practice are given in Section 4.2. Also, for the purpose of the discussion on plastic algorithms that follows in Section 4.2, it proves convenient to consider inviscid plasticity as a limiting case of viscoplasticity, as the viscosity tends to 0. In this indirect way, eq. (16) also encompasses the inviscid plasticity case. It is finally assumed that the evolution of the internal variables is governed by kinetic equations of the form

$$\overset{\circ}{\mathbf{q}} = \mathbf{f}(\boldsymbol{\sigma}, \mathbf{q}) \tag{17}$$

Note that the use of the Truesdell rate in the left hand side of (17) makes these equations objective and consistent with a set of material kinetic equations [18].

The spatial rate form of the constitutive equation (15) expresses the linear dependence of the Truesdell rate of Cauchy stress $\overset{\circ}{\boldsymbol{\sigma}}$ on the elastic part of the spatial deformation rate tensor $\mathbf{d}^e$ through the spatial elasticity tensor $\mathbf{a}$. It can be shown by use of a Legendre transformation [18] that $\mathbf{a}$ is a function only of the deformation and the internal variables. However, eq. (15) is expressible in terms of other stress rates if the difference between these rates and the Truesdell rate of Cauchy stress is absorbed in the definition of the elasticity tensor. In this case, the elasticity tensor will, in general, be a function of the stress tensor, the deformation and the internal variables [18].

3.3. Summary of Field Equations

For later reference, the field equations introduced above are summarized as follows

$$\begin{aligned}
\dot{\boldsymbol{\phi}}_t &= \mathbf{v} \circ \boldsymbol{\phi}_t \\
\rho\, \dot{\mathbf{v}} &= \nabla \cdot \boldsymbol{\sigma} + \rho\, \mathbf{b} \\
\overset{\circ}{\boldsymbol{\sigma}} &= \mathbf{a} : (\mathbf{d} - \mathbf{T}(\boldsymbol{\sigma}, \mathbf{q})) \\
\overset{\circ}{\mathbf{q}} &= \mathbf{f}(\boldsymbol{\sigma}, \mathbf{q}) \\
\boldsymbol{\sigma} \cdot \mathbf{n} &= \bar{\mathbf{t}} \qquad \mathbf{x} \in \partial_\sigma \boldsymbol{\phi}_t(B) \\
\boldsymbol{\phi} &= \bar{\boldsymbol{\phi}} \qquad \mathbf{x} \in \partial_u \boldsymbol{\phi}_t(B)
\end{aligned} \tag{18}$$

It is demonstrated in the next section that the field eqs. (18) admit an additive decomposition into elastic and plastic parts suggesting a global solution procedure based on the product formula algorithms discussed in Section 2. The product formula algorithm applied to this decomposition results in a step-by-step integration procedure in which a nonlinear elastodynamic problem is first solved, followed by the application of algorithms that bring in the plastic part of the evolutionary equations.

4. The Elastoplastic Split of the Dynamic Equations of Motion and Related Product Algorithms.

The field equations (18) exhibit an additive decomposition into an elastic part

$$\begin{aligned} \dot{\boldsymbol{\phi}}_t &= \mathbf{v}\circ\boldsymbol{\phi}_t \\ \rho\,\dot{\mathbf{v}} &= \nabla\cdot\boldsymbol{\sigma} + \rho\,\mathbf{b} \\ \overset{\circ}{\boldsymbol{\sigma}} &= \mathbf{a}:\mathbf{d} \\ \partial\mathbf{q}/\partial t &= 0 \\ \boldsymbol{\sigma}\cdot\mathbf{n} = \bar{\mathbf{t}} & \quad \mathbf{x}\in\partial_\sigma\boldsymbol{\phi}_t(B) \\ \boldsymbol{\phi} = \bar{\boldsymbol{\phi}} & \quad \mathbf{x}\in\partial_u\boldsymbol{\phi}_t(B) \end{aligned} \tag{19}$$

and a plastic part

$$\begin{aligned} \dot{\boldsymbol{\phi}}_t &= 0 \\ \rho\,\dot{\mathbf{v}} &= 0 \\ \partial\boldsymbol{\sigma}/\partial t &= -\mathbf{a}:\mathbf{T}(\boldsymbol{\sigma},\mathbf{q}) \\ \overset{\circ}{\mathbf{q}} &= \mathbf{f}(\boldsymbol{\sigma},\mathbf{q}) \end{aligned} \tag{20}$$

This suggests the possibility of using the product formula techniques to construct efficient numerical algorithms that exploit such additive decomposition. It is noted that eqs. (19) define a finite deformation elastodynamic problem, while the second set of eqs. (20) leaves the configuration unchanged and defines a pointwise relaxation process for stresses and internal variables.

In the present context, a product algorithm relative to the elastoplastic additive decomposition of the equations of motion takes the following meaning. Consider two unconditionally stable algorithms $\mathbf{F}^{el}(h)$ and $\mathbf{F}^{pl}(h)$ consistent with the individual equations (19) and (20) according to the discussion in Section 2. Given two such algorithms, an algorithm $\mathbf{F}(h)$ consistent with the full equations of motion (18) can be obtained by means of the product formula

$$\mathbf{F}(h) = \mathbf{F}^{pl}(h)\,\mathbf{F}^{el}(h) \tag{21}$$

It is recalled from Section 2 that $\mathbf{F}(h)$ is in fact consistent with (18) and that if the individual algorithms $\mathbf{F}^{el}(h)$ and $\mathbf{F}^{pl}(h)$ are unconditionally stable in the sense of (4) so is $\mathbf{F}(h)$.

The product formula (21) simply states that a solution algorithm for the elastoplastic problem can be obtained by solving for each time step an elastic dynamic problem first, and then applying to the solution vector so obtained a plastic algorithm operating on the stresses and internal variables bringing in the effect of the plastic constitutive equations. It is interesting to note that all the boundary value aspects of the elastoplastic dynamic problem are included in the elastic eqs. (19) and are taken care of by the elastic algorithm $\mathbf{F}^{el}(h)$.

In practice, the above equations are solved by means of some spatial discretization technique such as the finite element method. In this case, the plastic part of the equations of motion will correspond to a set of relaxation equations expressed at the integration points within the elements. Thus, the plastic algorithm $\mathbf{F}^{pl}(h)$ is applied integration point by integration point and amounts to solving eqs. (20) numerically or exactly at each one of them. In Section 4.2 several widely used plastic constitutive assumptions are considered, and the nature of the associated plastic algorithms and the resulting product formula solution schemes is reexamined for each case.

4.1. Algorithm for the Elastic Dynamic Problem

This Section is concerned with the development of an algorithm $\mathbf{F}^{el}(h)$ for the numerical solution of the elastic dynamic boundary value problem given by eqs. (19). A weak form of this problem is expressed by

$$\int_{\boldsymbol{\phi}_t(B)} [\rho\,(\dot{\mathbf{v}} - \mathbf{b})\cdot\boldsymbol{\eta} + \boldsymbol{\sigma} : \nabla\boldsymbol{\eta}]\, dv = \int_{\partial_\sigma \boldsymbol{\phi}_t(B)} \bar{\mathbf{t}}\cdot\boldsymbol{\eta}\, da \tag{22}$$

for all weighting functions $\boldsymbol{\eta}$ which satisfy the homogeneous boundary conditions on $\partial_u \boldsymbol{\phi}_t(B)$. Spatial discretization is accomplished using the finite element method for which a set of global finite element interpolation functions N_a, $a = 1,2, \cdots, n$ is introduced. The interpolated motion and weighting functions take the form $\boldsymbol{\phi} = \boldsymbol{\phi}^a N_a$ and $\boldsymbol{\eta} = \boldsymbol{\eta}^a N_a$, where the summation convention is implied and $\boldsymbol{\phi}^a$ and $\boldsymbol{\eta}^a$ denote the nodal values of $\boldsymbol{\phi}$ and $\boldsymbol{\eta}$, respectively. The global interpolation functions are given by the expression $N_a = \sum_{e=1}^{Nel} N_a^e$ where the index e ranges over the elements and N_a^e denotes the element interpolation functions. Using the above results in (22) one obtains the following spatially discretized weak form

$$\mathbf{M}\cdot\dot{\mathbf{v}} + \mathbf{P}(\boldsymbol{\sigma}, t) = \mathbf{F}(t) \tag{23}$$

where $\mathbf{M}$ is the mass matrix with components

$$M_{ab} = \sum_{e=1}^{Nel} \int_{\Omega^e} \rho \, N_a^e N_b^e \, d\Omega, \tag{24}$$

$\mathbf{P}(\sigma, t)$ is the "internal force" vector with components

$$\mathbf{P}_a = \sum_{e=1}^{Nel} \int_{\Omega^e} (\mathbf{B}_a^e)^T \cdot \sigma \, d\Omega \tag{25}$$

where $\mathbf{B}_a$ is a matrix involving spatial gradients of N_a, finally $\mathbf{F}$ is the global force vector with components

$$\mathbf{F}_a = \sum_{e=1}^{Nel} \left(\int_{\Omega^e} \rho \, \mathbf{b} \, N_a^e \, d\Omega + \int_{\partial\Omega_\sigma^e} \mathbf{t} N_a^e \, d\Gamma \right). \tag{26}$$

In eqs. (24), (25) and (26) Ω_e is a domain given by the current configuration of a finite element e such that $\bigcup_{e=1}^{Nel} \Omega^e = \phi_t(B)$ and $\bigcap_{e=1}^{Nel} \Omega^e = \emptyset$.

4.1.1. Temporal Integration of the Weak Form

The spatially discretized weak form (23) is integrated in time by the application of the implicit Newmark algorithm defined by

$$\mathbf{M} \cdot \dot{\mathbf{v}}_{n+1} + \mathbf{P}_{n+1}(\sigma_{n+1}) = \mathbf{F}_{n+1} \tag{27}$$

$$\phi_{n+1} = \phi_n + h\mathbf{v}_n + h^2[(\frac{1}{2} - \beta)\dot{\mathbf{v}}_n + \beta \dot{\mathbf{v}}_{n+1}] \tag{28}$$

$$\mathbf{v}_{n+1} = \mathbf{v}_n + h[(1-\gamma)\dot{\mathbf{v}}_n + \gamma \dot{\mathbf{v}}_{n+1}] \tag{29}$$

where subscripts n and $n+1$ denote variables evaluated at the nth and $n+1$th time steps, $h = t_{n+1} - t_n$ is the time step size and β and γ are the Newmark parameters. Substituting (28) and (29) into (27) results in

$$G(\phi_{n+1}) \equiv \frac{1}{\beta h^2} \mathbf{M} \cdot \phi_{n+1} + \mathbf{P}_{n+1}(\sigma_{n+1}) - \hat{\mathbf{P}}_{n+1} = 0 \tag{30}$$

where $\hat{\mathbf{P}}_{n+1} = \mathbf{F}_{n+1} - \mathbf{M} \cdot [(1 - \frac{1}{2\beta})\dot{\mathbf{v}}_n - \frac{1}{\beta h}\mathbf{v}_n - \frac{1}{\beta h^2}\phi_n]$. For this formulation $\beta \neq 0$. It is noted that the choice of $\beta = 0.25$ and $\gamma = 0.5$ corresponds to the trapezoidal rule.

In order to complete eq. (30) the elastic constitutive equation (19.c) must be introduced. However, since the rate constitutive eq.(19.c) is not directly integrable it is not possible to replace σ_{n+1} appearing in (30) directly in terms of the motion ϕ_{n+1}. In general eq. (30) together with (28) and (29) define a system of nonlinear equations whose solution can be obtained by consistent linearization and the application of a Newton Raphson iteration scheme. The next Section considers linearization of the weak form (30) consistent with the spatial rate constitutive equation (19.c).

4.1.2. Linearization of the Discretized Weak Form of Momentum Balance

Formally, it is found that a consistent linearization procedure may be based on Taylor's formula for C^1 functions [15,22]. Let A and B be Banach spaces and $\mathbf{f}: A \rightarrow B$ be a C^1 mapping and let $\mathbf{x}' \in A$. Then the linearization of $\mathbf{f}$ about $\mathbf{x}'$ is

$$L[\mathbf{f}, \mathbf{u}]_{\mathbf{x}'} = \mathbf{f}(\mathbf{x}') + \mathbf{Df}(\mathbf{x}') \cdot \mathbf{u} \tag{31}$$

for $\mathbf{u} \in A$. In (31) $\mathbf{Df}(\mathbf{x}')$ is the Frechet derivative of $\mathbf{f}$ evaluated at $\mathbf{x}'$ and can be computed from the definition of the directional derivative

$$\mathbf{Df}(\mathbf{x}') \cdot \mathbf{u} = \frac{d}{d\epsilon} \mathbf{f}(\mathbf{x}' + \epsilon \mathbf{u})|_{\epsilon=0} \tag{32}$$

In the sequel, $\mathbf{x}' \in A$ will be interpreted as a set of spatial coordinates of the body given by the mapping $\mathbf{x}' = \boldsymbol{\phi}'_t(\mathbf{X})$ and $\mathbf{u}: \boldsymbol{\phi}'_t(B) \rightarrow R^N$ will be interpreted as an infinitesimal deformation superimposed on the configuration $\boldsymbol{\phi}'_t(B)$.

If $\boldsymbol{\Gamma}$ is a tensor field defined on the reference configuration B then eq. (32) may be employed to obtain the directional derivative of $\boldsymbol{\Gamma}$ in the direction of the incremental motion $\mathbf{u}$, resulting in

$$\mathbf{D}\boldsymbol{\Gamma}(\mathbf{X}, t) \cdot \mathbf{u} = \frac{d}{d\epsilon} \boldsymbol{\Gamma}(\boldsymbol{\phi}_\epsilon^{-1}, t)|_{\epsilon=0} \tag{33}$$

where $\boldsymbol{\phi}_\epsilon = \epsilon \mathbf{u} \circ \boldsymbol{\phi}'_t : B \rightarrow R^N$. Using definition (33), it can be shown [18] that the directional derivative of the second Piola-Kirchhoff stress tensor $\mathbf{S}$ is associated with the Lie derivative of the Kirchhoff stress tensor $\boldsymbol{\tau}$ taken with respect to the incremental motion $\mathbf{u}$ such that

$$\mathbf{DS} \cdot \mathbf{u} = \boldsymbol{\phi}'^{*}_t [L_{\mathbf{u}}(\boldsymbol{\tau})] \tag{34}$$

where

$$L_{\mathbf{u}}(\boldsymbol{\tau}) = \frac{d}{d\epsilon} (\boldsymbol{\phi}_\epsilon \circ \boldsymbol{\phi}'^{-1}_t)^{*}(\boldsymbol{\tau})|_{\epsilon=0}$$

This result is useful for the linearization of the discretized weak form (30) which is considered next.

Applying definitions (31) and (32) to eq. (30) results in

$$L[G(\boldsymbol{\phi}'_{n+1})] = G(\boldsymbol{\phi}'_{n+1}) + \mathbf{D}G(\boldsymbol{\phi}'_{n+1}) \cdot \mathbf{u}_{n+1} = 0 \tag{35}$$

where

$$\mathbf{D}G(\boldsymbol{\phi}'_{n+1}) = \frac{1}{\beta h^2}\mathbf{M} \cdot \mathbf{u}_{n+1} + \mathbf{DP}_{n+1} \cdot \mathbf{u}_{n+1}. \tag{36}$$

In order to evaluate the directional derivative of $\mathbf{P}_{n+1}$ appearing in (36) consistent with the spatial rate constitutive equation (19.c) it is convenient to return to the weak form (22) and consider the part from which $\mathbf{P}_{n+1}$ is derived, namely

$$\sum_{e=1}^{Nel} \int_{\Omega^e} \boldsymbol{\sigma} : \nabla \boldsymbol{\eta}\, d\Omega = \int_{\boldsymbol{\phi}_t(B)} \boldsymbol{\sigma} : \nabla \boldsymbol{\eta}\, dv = \int_B tr(\mathbf{S} \cdot \mathbf{F}^T \cdot \nabla_0 \boldsymbol{\eta}_0)\, dV \tag{37}$$

where $\boldsymbol{\eta}_0 = \boldsymbol{\eta} \circ \boldsymbol{\phi}'_t$ and ∇_0 denotes the gradient with respect to the material coordinates X. Using (32) and (34) it may be shown [18] that

$$\mathbf{D}\left[\int_{\boldsymbol{\phi}_t(B)} \boldsymbol{\sigma} : \nabla \boldsymbol{\eta}\, dv\right] \cdot \mathbf{u} = \int_B tr([\mathbf{DS} \cdot \mathbf{u}] \cdot \mathbf{F}^T \cdot \nabla_0 \boldsymbol{\eta}_0 + \mathbf{S} \cdot [\nabla_0 \mathbf{u} \circ \boldsymbol{\phi}'_t]^T \cdot \nabla_0 \boldsymbol{\eta}_0)\, dV$$

$$= \int_{\boldsymbol{\phi}_t(B)} tr[(\boldsymbol{\sigma} \cdot \nabla \mathbf{u}^T + J^{-1} L_{\mathbf{u}}(\boldsymbol{\tau})) \cdot \nabla \boldsymbol{\eta}]\, dv. \tag{38}$$

Using (9) and the hyperelastic constitutive equation (19.c), i.e. $\overset{\circ}{\boldsymbol{\sigma}} = J^{-1} L_{\mathbf{v}}(\boldsymbol{\tau}) = \mathbf{a} : \mathbf{d}$ leads to the approximation

$$J^{-1} L_{\mathbf{u}}(\boldsymbol{\tau}) = \mathbf{a} : \nabla^S \mathbf{u}. \tag{39}$$

Substitution of (39) into (38) results in

$$\mathbf{DP}_{n+1} \cdot \mathbf{u}_{n+1} = \sum_{e=1}^{Nel} \int_{\Omega^e} (\mathbf{B}_a^e)^T \cdot (\boldsymbol{\sigma} \cdot \nabla \mathbf{u}^T + \mathbf{a} : \nabla^S \mathbf{u})|_{n+1}\, d\Omega \tag{40}$$

It follows from (35), (36) and (40) that the linearization of (30) is given by

$$\frac{1}{\beta h^2}\mathbf{M} \cdot \mathbf{u}^i_{n+1} + \int_{\boldsymbol{\phi}^i_{n+1}(B)} \mathbf{B}^T \cdot (\boldsymbol{\sigma} \cdot \nabla \mathbf{u}^T + \mathbf{a} : \nabla^S \mathbf{u})|^i_{n+1}\, dv = -G(\boldsymbol{\phi}^i_{n+1}) \tag{41}$$

where $\boldsymbol{\phi}'_t$ in (35) has been replaced by $\boldsymbol{\phi}^i_{n+1}$ to represent an iterative solution procedure in which superscript i denotes the iteration counter. Equation (41) is linear in the incremental motion $\mathbf{u}^i_{n+1}$. Updating of the motion is accomplished by setting

$$\boldsymbol{\phi}_{n+1}^{i+1} = \boldsymbol{\phi}_{n+1}^{i} + \mathbf{u}_{n+1}^{i} \tag{42}$$

However, updating of the stress tensor corresponding to $\boldsymbol{\phi}_{n+1}^{i+1}$ is achieved by integration of the spatial rate constitutive equation (19.c), the subject of the next section.

4.1.3. Numerical Integration of Hyperelastic Rate Constitutive Equations

From a numerical point of view, an algorithm for the integration of rate constitutive equations should satisfy three requirements:

(a) Consistency with the constitutive equations.

(b) Numerical stability.

(c) Incremental objectivity.

Conditions (a) and (b) are required for the convergence of the numerical integration scheme [3]. The condition of incremental objectivity is a physical requirement expressing the fact that the algorithm has to be invariant with respect to superimposed rigid body motions. This notion was first formalized in an algorithmic context in [20]. More recently, a family of computationally efficient algorithms satisfying the requirements of consistency, numerical stability and incremental objectivity has been proposed in [28]. These algorithms fit naturally into a finite element implementation of the problem since they employ quantities that are readily available in such a context. This integration scheme applies equally well for any choice of objective stress rate appearing in the constitutive equations.

The algorithmic problem can be stated as follows. It is assumed that at time t_n the configuration $\boldsymbol{\phi}_n(B)$, denoted $\boldsymbol{\Omega}_n$, and the stress tensor $\boldsymbol{\sigma}_n$ at each material point in $\boldsymbol{\Omega}_n$ is known. At time t_{n+1}, the continuum occupies the known configuration $\boldsymbol{\phi}_{n+1}(B)$, denoted $\boldsymbol{\Omega}_{n+1}$. The problem is to determine the corresponding $\boldsymbol{\sigma}_{n+1}$ at each point in $\boldsymbol{\Omega}_{n+1}$.

In the past, some implicit numerical integration schemes applied to spatial rate constitutive equations have employed difference operations on the spatial stress components of the form $[\sigma_{n+1}^{ij} - \sigma_n^{ij}]$. However, such quantities are of limited value. From a mathematical point of view, the usual linear space operations such as addition and scalar multiplication can only be rigorously applied to relate tensor fields associated with a common configuration.* These considerations lead naturally to the idea of pulling back spatial quantities to a common reference configuration in order to define difference operators to be used in numerical algorithms. Recalling that the second Piola-Kirchhoff stress tensor is the backward Piola transformation of the Cauchy stress tensor (or, alternatively, the pull back of the Kirchhoff stress), the above discussion suggests defining algorithms for the integration of the spatial rate constitutive equations based upon difference operators employing the second Piola-Kirchhoff stress tensor. For example, a generalized midpoint rule algorithm for the spatial rate constitutive equations can be introduced as follows

$$\mathbf{S}_{n+1} - \mathbf{S}_n = h\,\dot{\mathbf{S}}_{n+\alpha} \qquad 0 \leqslant \alpha \leqslant 1 \tag{43}$$

where $h = t_{n+1} - t_n$ and $\dot{\mathbf{S}}_{n+\alpha}$ will be evaluated on an intermediate configuration $\Omega_{n+\alpha}$ defined as

$$\boldsymbol{\phi}_{n+\alpha} = \alpha\boldsymbol{\phi}_{n+1} + (1-\alpha)\,\boldsymbol{\phi}_n \quad 0 \leqslant \alpha \leqslant 1 \tag{44}$$

Using (8) and noting that $\mathbf{S} = J\boldsymbol{\phi}_t^{*}(\boldsymbol{\sigma})$, (43) has the alternative representation

$$\boldsymbol{\phi}^{*}_{n+1}(J\boldsymbol{\sigma}) - \boldsymbol{\phi}^{*}_{n}(J\boldsymbol{\sigma}) = h\,\boldsymbol{\phi}^{*}_{n+\alpha}(\overset{\circ}{J\boldsymbol{\sigma}}) \tag{45}$$

In reference to the comments above, it is noted that quantities involved in (45) are all referred to a common configuration.

To simplify (45) it is advantageous to select the reference configuration B to coincide instantaneously with Ω_{n+1} [28], in which case (45) reduces to

$$\boldsymbol{\sigma}_{n+1} - \boldsymbol{\phi}^{*}_{n}(J\boldsymbol{\sigma}) = h\,\boldsymbol{\phi}^{*}_{n+\alpha}(\overset{\circ}{J\boldsymbol{\sigma}}) \tag{46}$$

Defining the deformation gradients

$$\boldsymbol{\Lambda}_{n+\alpha} = \left(\frac{\partial\boldsymbol{\phi}_{n+\alpha}}{\partial\mathbf{x}_{n+1}}\right)^{-1} \quad 0 \leqslant \alpha \leqslant 1 \tag{47}$$

and Jacobians

* The set of all configurations of a body can be shown to be a smooth manifold [17]. Each configuration of the body defines a point in this manifold. A tensor field defined on a particular configuration is a member of the tangent space associated with that configuration. Therefore, tensor fields defined on different configurations belong to different linear spaces and cannot be combined by means of the usual linear space operations such as addition and subtraction.

$$J_{n+\alpha} = \det(\mathbf{\Lambda}_{n+\alpha}) \quad 0 \leqslant \alpha \leqslant 1 \tag{48}$$

then, for contravariant components of stress, (46) has the form

$$\boldsymbol{\sigma}_{n+1} - J_n^{-1} \mathbf{\Lambda}_n \cdot \boldsymbol{\sigma}_n \cdot \mathbf{\Lambda}_n^T = h\, J_{n+\alpha}^{-1} \mathbf{\Lambda}_{n+\alpha} \cdot \overset{\circ}{\boldsymbol{\sigma}}_{n+\alpha} \cdot \mathbf{\Lambda}_{n+\alpha}^T \tag{49}$$

This equation is completed by introducing the rate constitutive equation for $\overset{\circ}{\boldsymbol{\sigma}}_{n+\alpha}$. For example, for constitutive eq. (19.c), eq. (49) is expressed by

$$\boldsymbol{\sigma}_{n+1} - J_n^{-1} \mathbf{\Lambda}_n \cdot \boldsymbol{\sigma}_n \cdot \mathbf{\Lambda}_n^T = h\, J_{n+\alpha}^{-1} \mathbf{\Lambda}_{n+\alpha} \cdot (\mathbf{a} : \mathbf{d})_{n+\alpha} \cdot \mathbf{\Lambda}_{n+\alpha}^T \tag{50}$$

This form requires the evaluation of quantities $\mathbf{\Lambda}_{n+\alpha}$ and $\mathbf{d}_{n+\alpha}$. It is shown in [28] that $\mathbf{\Lambda}_{n+\alpha}$ is given by

$$\mathbf{\Lambda}_{n+\alpha} = [(1-\alpha)\,\mathbf{I} + \alpha\,\mathbf{\Lambda}_n]^{-1} \cdot \mathbf{\Lambda}_n$$

and that $\mathbf{d}_{n+\alpha}$ is consistently approximated by

$$\mathbf{d}_{n+\alpha} = \frac{1}{h}\left[\left\{(1-\alpha)\mathbf{I} + \alpha\mathbf{\Lambda}_n\right\}^{-1}\left\{\mathbf{\Lambda}_n - \mathbf{I}\right\}\right]^S$$

As noted above, from a numerical point of view, the proposed algorithm has to satisfy the three requirements of consistency with the spatial rate constitutive equations, numerical stability and incremental objectivity. It is shown in [28] that the above algorithm is consistent with the rate constitutive equation and that it is unconditionally stable for $\alpha \geqslant 0.5$, moreover, it is second order accurate for $\alpha = 0.5$. The condition of incremental objectivity is a physical requirement expressing the fact that the algorithm has to be invariant with respect to superimposed rigid body motions occurring over the time step. It is shown in [28] that such a requirement is satisfied if and only if α is restricted to the value of 0.5.

The algorithm (50) may be generalized to accommodate choices of objective stress rate other than the Truesdell rate of Cauchy stress by embedding the difference between the stress rate definitions into $\mathbf{a}$. In this case (50) will, in general, become implicit in $\boldsymbol{\sigma}_{n+1}$ and may be solved by means of an iterative solution procedure [28].

A numerical example will serve to illustrate the accuracy and incremental objectivity of the algorithm. The problem considered is the homogeneous finite simple extension (i.e. with restrained Poisson effect) and simultaneous rigid rotation of a rectangular block. The constitutive equation employed to test the algorithm was taken to be $\overset{\nabla}{\tau} = \mathbf{a} : \mathbf{d}$ where $a_{ijkl} = \lambda\delta_{ij}\delta_{kl} + \mu(\delta_{ik}\delta_{jl} + \delta_{il}\delta_{jk})$ and λ, μ are constants. This constitutive equation is adopted only for the purpose of testing the integration algorithm. Referring to Fig. 1 and noting that $\theta(t)$ represents rigid rotation of the block at time t and $\lambda(t)$ the axial stretch ratio (in the rotated coordinated frame), the analytical solution for two of the stress components (relative to the fixed spatial coordinate system) for a unit cube is given by [18]

$$\begin{Bmatrix} \tau_{11} \\ \tau_{22} \end{Bmatrix} = \begin{bmatrix} \cos^2\theta & \sin^2\theta \\ \sin^2\theta & \cos^2\theta \end{bmatrix} \begin{Bmatrix} 1 \\ \dfrac{\nu}{1-\nu} \end{Bmatrix} \frac{E(1-\nu)}{(1+\nu)(1-2\nu)} \ln\lambda$$

The time dependence of the kinematic variables defining the problem is prescribed as

$$\theta(t) = 2\pi t \quad \text{and} \quad \lambda(t) = 1 + t \qquad \text{for} \quad 0 \leqslant t \leqslant 1$$

Thus, the cube is stretched to double its length and simultaneously rotated through 360 degrees. The solid curves of Fig. 1 depict the analytical solutions for this combination of θ and λ.

The numerical solution was obtained by discretization of the block into four quadrilateral plane strain finite elements. The mesh is shown in Fig. 1. The analysis was performed in the fixed spatial coordinate system with the θ and λ deformation states imposed by suitable prescription of the boundary node displacements. The numerical integration algorithm employed the iterative solution procedure mentioned above since it is implicit for the given constitutive equation. The stress components resulting from the analysis are shown as dots in Fig. 1. They display accuracy to within 0.1% of the analytical solution over the full range of deformation. Convergence was obtained for the problem using as few as ten equal increments of (θ,λ). This analysis tends to confirm the incremental objectivity of the numerical solution procedure.

4.2. Plastic Algorithms and Associated Product Formulas for Perfect and Hardening Plasticity and Viscoplasticity.

The algorithm for the solution of the nonlinear elastodynamic problem given by eq. (19) discussed above can be expressed as

$$\mathbf{F}^{el}(h)\begin{Bmatrix}\phi_n^e\\ \sigma_n^{e,k}\end{Bmatrix} = \begin{Bmatrix}\phi_{n+1}^e\\ \sigma_{n+1}^{e,k}\end{Bmatrix}$$

where $\sigma_{n+1}^{e,k}$ denotes the value of the solution particularized for integration point k in element e.

This section is concerned with the development of plastic algorithms $\mathbf{F}^{pl}(h)$ for the solution of the plastic part of the field equations eqs. (20). These relaxation equations often admit closed form solutions that are readily obtained and which can be used directly in the plastic algorithm. In this case, a necessary and sufficient condition for $\mathbf{F}^{pl}(h)$ to be unconditionally stable in the sense of (4) is that the plastic eqs. (20) be "dissipative" [34], i.e.,

$$-\,\sigma:\mathbf{T}(\sigma,\mathbf{q}) = \sigma:\mathbf{d}^p \geqslant (\mathbf{q},\mathbf{f}(\sigma,\mathbf{q})) = (\mathbf{q},\dot{\mathbf{q}})$$

where $(\cdot,\cdot)$ indicates some appropriate inner product for the internal variables. This dissipativity condition is satisfied by all models of practical interest*. Four examples of the plastic constitutive mappings appearing in (20) i.e. $\mathbf{T}(\sigma,\mathbf{q})$ and $\mathbf{f}(\sigma,\mathbf{q})$ are given. For simplicity of presentation, inviscid plasticity is considered as a limiting case of viscoplasticity, as the viscosity is allowed to tend to zero. A detailed mathematical discussion regarding product formula techniques for the solution of the elastoplastic and viscoplastic dynamic boundary value problems can be found in [33].

4.2.1. Perfect Viscoplasticity.

Consider a convex set C in stress space $S \equiv R^6$ containing the origin. Then, given any point σ in S, there is always one and only one point $\mathbf{P}_C\sigma$ in C which is closest to σ [5,6].

* In fact, if the quantity $\chi(\sigma,\mathbf{q}) = \frac{1}{2}\sigma{:}\mathrm{C}{:}\sigma + \sigma{:}\epsilon^p - \frac{1}{2}(\mathbf{q},\mathbf{q})$ is taken as the complementary free energy potential, then the above dissipativity condition is simply a statement of the Clausius-Plank dissipation inequality.

The mapping $\mathbf{P}_C$ is called the closest point mapping (relative to C). Clearly, if σ is a point in C then $\mathbf{P}_C\sigma = \sigma$.

For a perfectly viscoplastic material, the existence of one such closed convex set C is assumed such that the plastic constitutive mapping $\mathbf{T}(\sigma)$ is given by

$$\mathbf{d}^p = \frac{\sigma - \mathbf{P}_C\sigma}{\eta} = \mathbf{T}(\sigma) \tag{51}$$

The parameter η is the viscosity of the material. Note that no internal variables are needed in this model.

It is interesting to note that $\mathbf{T}$ is defined regardless of the smoothness of C, given that the closest point mapping is always well-defined for every closed convex set C [5,6]. If σ belongs to C then $\mathbf{P}_C\sigma = \sigma$ and $\mathbf{d}^p = 0$. If, on the other hand, σ does not belong to C then $\mathbf{d}^p$ is directed along the vector that joins σ and its closest point in C and it points outside the elastic region. The magnitude of $\mathbf{d}^p$ is proportional to the distance from σ to C, the proportionality constant being $\frac{1}{\eta}$, Fig. 2.

For this specific model, the relaxation eqs. (20) at a generic integration point take the form

$$\dot{\sigma} = -\mathbf{a}:\mathbf{T}(\sigma) = -\mathbf{a}:\frac{\sigma - \mathbf{P}_C\sigma}{\eta} \tag{52}$$

This is a system of ordinary differential equations whose solution is

$$\begin{aligned} &\sigma(t) = \sigma_o \qquad \textit{if } \sigma_o \in C \\ &\sigma(t) = \exp(-\mathbf{a}\, t/\eta):\sigma_o + [\mathbf{I} - \exp(-\mathbf{a}\, t/\eta)]:\mathbf{P}_C\sigma_o \qquad \textit{otherwise} \end{aligned} \tag{53}$$

For the familiar case of isochoric plasticity in which C is a cylinder oriented along the hydrostatic axis and for isotropic elasticity, eq. (53.b) simplifies to

$$\begin{aligned} \sigma(t) &= e^{-t/\tau}\sigma_o + (1 - e^{-t/\tau})\,\mathbf{P}_C\sigma_o \\ &= p_o\mathbf{I} + e^{-t/\tau}\mathbf{s}_o + (1 - e^{-t/\tau})\,\mathbf{P}_C\mathbf{s}_o \end{aligned} \tag{54}$$

where $p_o = \sigma_o:\mathbf{I}$ is the initial hydrostatic pressure and $\tau = \eta/G$ is the relaxation time of the process, given in terms of the shear modulus of the material G.

For instance, for the von Mises yield criterion the elastic domain C is the set $\{\sigma \in S$ *such* *that* $J_2 \leq k^2\}$, where k is the shear yield stress, $J_2 = \frac{1}{2}\mathbf{s}{:}\mathbf{s}$ and $\mathbf{s}$ is the deviatoric part of $\boldsymbol{\sigma}$. In this particular instance, eq. (54) reduces to

$$\boldsymbol{\sigma}(t) = p_o \mathbf{I} + e^{-t/\tau}\mathbf{s}_o + (1 - e^{-t/\tau})\frac{k}{r_o}\mathbf{s}_o \tag{55}$$

where $r_o = \sqrt{\frac{1}{2}\mathbf{s}_o{:}\mathbf{s}_o}$.

Clearly, the simplest possible choice of plastic algorithm for this specific model consists of using the solution of the relaxation equations (53). This algorithm can be expressed

$$\mathbf{F}^{pl}(h)\begin{Bmatrix}\boldsymbol{\phi}_i^e\\ \boldsymbol{\sigma}^{e,k}\end{Bmatrix} = \begin{Bmatrix}\boldsymbol{\phi}_i^e\\ \boldsymbol{\sigma}^{e,k}(h)\end{Bmatrix} \tag{56}$$

where $\boldsymbol{\sigma}^{e,k}(h)$ denotes the value of the solution (53) (or (54) and (55) when applicable) particularized for integration point k in element e, initial conditions $\boldsymbol{\sigma}_o = \boldsymbol{\sigma}^{e,k}$ and $t=h$.

The resulting product algorithm (21) then consists of first solving an incremental elastic problem, with time step h, ignoring the plasticity of the material. The stresses resulting from this operation are then allowed to relax at each integration point according to (53) for a period of time h, Fig. 3. Clearly, the stresses resulting from the application of the elastic algorithm that lie inside the elastic region are unaffected by this relaxation process. We finally note that the dissipativity condition discussed in Section 4.2 here reduces to $\boldsymbol{\sigma}:\mathbf{d}^p \geq 0$ which is always satisfied provided C contains the origin. Consequently, the plastic algorithm (56) is unconditionally stable. The unconditional stability of the product algorithm then results provided the elastic algorithm is also unconditionally stable.

4.2.2. Perfect Plasticity.

For a perfectly plastic material, the plastic constitutive mapping is given by

$$\mathbf{d}^p = \mathbf{T}(\boldsymbol{\sigma}) \equiv \begin{cases}\lambda\,\mathbf{N} & \textit{if}\ \boldsymbol{\sigma} \in \partial C\\ 0 & \textit{if}\ \boldsymbol{\sigma} \in \textit{Int}\ C\end{cases} \tag{57}$$

where $\mathbf{N}$ denotes the normal to ∂C at $\boldsymbol{\sigma}$ and λ is a positive parameter but otherwise indeterminate. This definition presupposes the smoothness of the yield surface ∂C. For arbitrary elastic domains, $\lambda\,\mathbf{N}$ has to be replaced by the normal cone at $\boldsymbol{\sigma}$, Fig. 2. In any case, it is clear that the resulting constitutive mapping $\mathbf{T}$ is not single valued. This situation is commonly encountered in the theory of nonlinear equations of evolution [34] and can be handled with relative ease with the aid of mathematical tools such as subdifferential calculus [33]. For simplicity, however, a simpler way around is taken below, namely that of considering perfect plasticity as a limiting case of perfect viscoplasticity as $\eta \to 0$. Alternatively, one may think of this limiting process as the result of allowing an infinite period of time to elapse for the relaxation of the stresses towards the elastic region. Taking this limit on the viscoplastic algorithm (56) the following plastic algorithm is obtained for the perfect plasticity case

$$\mathbf{F}^{pl}(h)\begin{Bmatrix}\boldsymbol{\phi}_I^e \\ \boldsymbol{\sigma}^{e,k}\end{Bmatrix} \equiv \begin{Bmatrix}\boldsymbol{\phi}_I^e \\ \boldsymbol{\sigma}^{e,k}(\infty)\end{Bmatrix} = \begin{Bmatrix}\boldsymbol{\phi}_I^e \\ \mathbf{P}_{C^{e,k}}\boldsymbol{\sigma}^{e,k}\end{Bmatrix} \tag{58}$$

where $C^{e,k}$ denotes the elastic domain at integration point e,k and $\mathbf{P}_{C^{e,k}}$ denotes the closest point projection onto $C^{e,k}$. Clearly, if at some given integration point the stresses $\boldsymbol{\sigma}^{e,k}$ lie inside $C^{e,k}$ then they remain unaffected by the plastic algorithm. Algorithm (58) applies equally well to any closed convex elastic domain, regardless of the smoothness of the yield surface. Also note the independence of (58) from h and η, which is a manifestation of the rate independent nature of the perfect plasticity constitutive equations. For instance, for the von Mises yield criterion one obtains from (55)

$$\boldsymbol{\sigma}^{e,k}(\infty) = \mathbf{P}_{C^{e,k}}\boldsymbol{\sigma}^{e,k} = \begin{cases}\boldsymbol{\sigma}^{e,k} & \textit{if } r^{e,k} \leqslant k^{e,k} \\ p^{e,k}\mathbf{I} + \dfrac{k^{e,k}}{r^{e,k}}\mathbf{s}^{e,k} & \textit{otherwise}\end{cases} \tag{59}$$

where $k^{e,k}$ denotes the shear yield stress at integration point e,k, $p^{e,k}$ and $\mathbf{s}^{e,k}$ the hydrostatic pressure and the deviatoric part of $\boldsymbol{\sigma}^{e,k}$ and $r^{e,k} = (\frac{1}{2}\mathbf{s}^{e,k}{:}\mathbf{s}^{e,k})^{1/2}$.

The resulting product algorithm entails, as before, the solution of an incremental elastic problem first, ignoring the plasticity of the material. The stresses resulting from this operation are then projected at each integration point onto their closest points on the elastic domain. Clearly, this projection only alters the stresses lying outside the elastic region.

Naturally, the heuristic argument that has been followed to derive (58) requires mathematical proof. This however is beyond the scope of this paper. A rigorous mathematical treatment of the viscoplastic approximation to the elastic-perfectly plastic dynamic boundary value problem can be found in [33]. It is also shown in [33] how product formulas for the elastic-perfectly plastic problem can be treated directly without resorting to the viscoplastic limit.

It is noted that the closest point mapping in (58) can be viewed as an instance of the concept of "return mapping" discussed in [29,30,31,32] for the particular case of static problems and von Mises yield criterion. Certainly, the closest point mapping does not exhaust all the possible choices of return mapping that can be used to project stresses back to the elastic domain. A set of conditions on the return mapping have been presented in [33] that guarantee the consistency of the resulting plastic algorithm. The closest point mapping, however, stems naturally out of the geometry of the problem and has the widest possible range of applicability.

We finally recall a basic inequality regarding the closest point mapping for closed convex sets [6]

$$||\mathbf{P}_C\sigma_1 - \mathbf{P}_C\sigma_2|| \leqslant ||\sigma_1 - \sigma_2|| \qquad \textit{for all } \sigma_1,\sigma_2 \in S \tag{60}$$

This inequality states that the closest point mapping is contractive for any closed convex set C, and therefore the plastic algorithm (58) is always unconditionally stable, by definition (4). This also follows from the unconditional stability of the perfect viscoplasticity plastic algorithm shown in the preceding section, given that the perfectly plastic algorithm is just a limiting case of the viscoplastic one. Consequently, the product algorithm (21) is unconditionally stable, provided the elastic algorithm is also unconditionally stable.

4.2.3. Hardening Viscoplasticity

In the case of hardening viscoplasticity, the elastic domain $C(\mathbf{q})$ depends on the current value of the internal variables. The plastic constitutive equations then take the form

$$\begin{aligned} \mathbf{d}^p &= \frac{\sigma - \mathbf{P}_{C(\mathbf{q})}\sigma}{\eta} \equiv \mathbf{T}(\sigma,\mathbf{q}) \\ \dot{\mathbf{q}} &= \mathbf{f}(\sigma,\mathbf{q}) \end{aligned} \tag{61}$$

where $\mathbf{P}_{C(\mathbf{q})}$ denotes the closest point mapping relative to $C(\mathbf{q})$. The relaxation equations (20) then become, for a generic integration point

$$\begin{aligned} \dot{\sigma} &= -\,\mathbf{a} : \frac{\sigma - \mathbf{P}_{C(\mathbf{q})}\sigma}{\eta} \\ \dot{\mathbf{q}} &= \mathbf{f}(\sigma,\mathbf{q}) \end{aligned} \tag{62}$$

A specific example is furnished by the von Mises yield criterion with isotropic bilinear hardening and isotropic elasticity

$$\begin{aligned} \dot{\sigma} &= -\,2G\,\mathbf{d}^p = \frac{-\,G < \sqrt{J_2} - k >}{\eta}\,\frac{\mathbf{s}}{\sqrt{J_2}} \\ \dot{k} &= 2H\,(\frac{1}{2}\,\mathbf{d}^p : \mathbf{d}^p)^{1/2} = H\,\frac{< \sqrt{J_2} - k >}{\eta} \end{aligned} \tag{63}$$

where H denotes the shear plastic modulus. The solution of (63) is readily found to be

$$\begin{aligned} &\sigma(t) = \sigma_o \quad , \quad k(t) = k_o \quad , \quad \textit{if } r_o \leqslant k_o \\ &\left.\begin{aligned} \sigma(t) &= \sigma_o - \frac{\tau}{\tau_s}\,(r_o - k_o)\,(1 - e^{-t/\tau})\,\frac{\mathbf{s}_o}{r_o} \\ k(t) &= k_o + \frac{\tau}{\tau_q}\,(r_o - k_o)\,(1 - e^{-t/\tau}) \end{aligned}\right. \quad \textit{otherwise} \end{aligned} \tag{64}$$

where

$$\tau_s = \frac{\eta}{G} \quad ; \quad \tau_q = \frac{\eta}{H} \quad ; \quad \tau = \frac{\tau_s\,\tau_q}{\tau_s + \tau_q} \tag{65}$$

are relaxation times for the process. It is seen from (64) that during a relaxation process corresponding to initial stresses outside the elastic domain, the stresses steadily approach the elastic domain, which at the same time expands towards the stress point.

As in the case of perfect viscoplasticity, the closed form solution (64) can be utilized to define plastic algorithms through

$$\mathbf{F}^{pl}(h) \begin{Bmatrix} \phi_i^e \\ \sigma^{e,k} \\ \mathbf{q}^{e,k} \end{Bmatrix} = \begin{Bmatrix} \phi_i^e \\ \sigma^{e,k}(h) \\ \mathbf{q}^{e,k}(h) \end{Bmatrix} \tag{66}$$

where $\sigma^{e,k}(h)$ and $\mathbf{q}^{e,k}(h)$ are given by (64) particularized for integration point e,k, initial conditions $\sigma_o = \sigma^{e,k}$, $\mathbf{q}_o = \mathbf{q}^{e,k}$ and $t = h$. In this case, however, not only do the stresses at the integration points vary upon the application of the plastic algorithm but so do the internal variables and, as a result, the elastic domains.

Taking as inner product for the internal variables $(\mathbf{q}_1, \mathbf{q}_2) \equiv \frac{1}{2H} k_1 k_2$, the dissipativity condition is readily checked, which in turn implies the unconditional stability of the corresponding plastic algorithm. Therefore, once again the unconditional stability of the product algorithm (21) follows provided the elastic algorithm is unconditionally stable. The further case of kinematic hardening has also been treated in [8].

4.2.4. Hardening Plasticity.

As in the case of perfect plasticity, plastic algorithms for the hardening case can be obtained from (66) by taking the limit $\eta \to 0$, which leads to the expression

$$\mathbf{F}^{pl}(h) \begin{Bmatrix} \boldsymbol{\phi}_i^e \\ \boldsymbol{\sigma}^{e,k} \\ \mathbf{q}^{e,k} \end{Bmatrix} = \begin{Bmatrix} \boldsymbol{\phi}_i^e \\ \boldsymbol{\sigma}^{e,k}(\infty) \\ \mathbf{q}^{e,k}(\infty) \end{Bmatrix} \tag{67}$$

Here, the asymptotic values $\boldsymbol{\sigma}^{e,k}(\infty)$ and $\mathbf{q}^{e,k}(\infty)$ can be obtained from (64)

$$\begin{aligned} &\boldsymbol{\sigma}(\infty) = \boldsymbol{\sigma}_o \quad , \quad k(\infty) = k_o \quad \textit{if } r_o \leqslant k_o \\ &\left.\begin{aligned} \boldsymbol{\sigma}(\infty) &= \boldsymbol{\sigma}_o - \frac{G}{G+H}(r_o - k_o)\frac{\mathbf{s}_o}{r_o} \\ k(\infty) &= k_o + \frac{H}{G+H}(r_o - k_o) \end{aligned}\right\} \quad \textit{otherwise} \end{aligned} \tag{68}$$

for the von Mises, isotropic hardening case. Note that these limiting values are independent of η.

Eq. (68) yields a suitable "return mapping" for the isotropic hardening rule. It is seen from (68) that the stress point and the yield surface meet at some intermediate point on the segment joining their initial values, the distances from these being proportional to G and H, respectively. A similar geometric interpretation can be derived for the return mapping corresponding to the kinematic hardening rule [8]. Note that the perfectly plastic case is recovered by setting $H = 0$.

Finally, the unconditional stability of the plastic algorithm induced by this return mapping follows from that of the corresponding viscoplastic case. Consequently, the unconditional stability of the product algorithm (21) follows also, provided the elastic algorithm is unconditionally stable.

5. Numerical Examples

A number of examples are presented to illustrate the effectiveness of the algorithms described above. The first example concerns the deformation of an infinitely long (plane strain) internally pressurized thick walled cylinder. The tube was discretized by means of quadrilateral elements, with 16 elements across the thickness. For perfect plasticity employing the von Mises yield criterion, Fig. 4 depicts the hoop and radial stress in the tube for an internal pressure corresponding to a plastification of 75% of the wall thickness. The three curves illustrate the rate of convergence of the method as the number of load increments taken to reach the final pressure is increased. It is observed that a small number of load increments (6) results in reasonable accuracy. For 100 load increments the solution obtained is virtually identical to the exact solution [16]. Fig. 5 shows the distribution of all stress components at various stages of the plastification of the wall which are in good agreement with the analytical solution [16].

Fig. 6 shows results corresponding to the infinitesimal deformation of an internally pressurized disk (plane stress) for the case of perfect plasticity and the Tresca yield criterion. The exact analytical solutions are compared in the same figure against the numerical solutions which for the load increment selected display an accuracy comparable to that obtained in the purely elastic solution. This example emphasizes the applicability of the proposed algorithm to the case of yield surfaces that exhibit corners.

The next example shown in Fig. 7 illustrates the effect of viscosity. Again the infinitely long thick walled tube is considered, in this case for a perfectly viscoplastic material with a von Mises yield surface. All curves correspond to an internal pressure resulting in a plastification of 50% of the wall thickness and depict the effect of varying viscosities. The figures clearly display the inviscid limit obtained by decreasing the viscosity to zero. The curves representing this limiting case are identical to those reported for perfect plasticity, Fig. 5.

The final example concerns the finite deformation of the infinitely long, internally pressurized thick walled cylinder. The material behavior was taken to be isotropic hardening plasticity with a plastic hardening modulus H corresponding to 10% of the Young's modulus, Fig. 8. As discussed in Section 4.2.4, the plastic algorithm for this problem makes use of a return mapping which simultaneously accounts for the evolution of the elastic domain. Fig. 8 depicts the hoop stress through the wall thickness for 12 prescribed inner radial displacements. The maximum load result shown in Fig. 8 (curve 12), which corresponds to a 12% increase in the internal radius of the tube, was obtained in 24 equal displacement increments with each increment requiring approximately 5 Newton-Raphson iterations as described in Section 4.1.2.

Acknowledgements

Grants for the support of this work from the Lawrence Livermore National Laboratory and General Motors Research Laboratories are gratefully acknowledged.

References

1. M. Ortiz, P.M. Pinsky and R.L. Taylor, "Unconditionally Stable Element-by-Element Algorithms For Dynamic Problems," *Computer Methods in Applied Mechanics and Engineering,* (to appear).

2. T.J.R. Hughes, I. Levit and J. Winget, "Unconditionally Stable Element-by-Element Implicit Algorithms for Heat Conduction Analysis", *J. Engng. Mechs. Div. of ASCE,* (to appear).

3. G.W. Gear, **Numerical Initial Value Problems in Ordinary Differential Equations,** Prentice-Hall, 1971.

4. R.M. McMeeking and J. R. Rice, "Finite Element Formulations for Problems of Large Elastic-Plastic Deformation," *Int. J. Solids Struct., 11,* 601 (1975).

5. R.T. Rockafellar, *Convex Analysis,* Princeton University Press, 1970.

6. E.H. Zarantonello, "Projections on Convex Sets in Hilbert Space and Spectral Theory," in: E.H. Zarantonello (Ed.), *Symposium on Nonlinear Functional Analysis,* Academic Press, 237-424, 1971.

7. J.R. Osias and J. L. Swedlow, "Finite Elasto-Plastic Deformation - I. Theory and Numerical Examples," *Int. J. Solids Struct., 10,* 321 (1974).

8. M. Ortiz, P.M. Pinsky and R.L. Taylor, "Operator Split Methods for the Numerical Solution of the Elastoplastic Dynamic Problem," *Computer Methods in Applied Mechanics and Engineering,* (to appear).

9. J. Lubliner, "A Simple Theory of Plasticity," *Int. J. Solids Struct., 10,* 313-319 (1974).

10 B.D. Coleman and W. Noll, "The Thermodynamics of Elastic Materials with Heat Conduction and Viscosity," *Arch. Ration. Mech. Anal., 13,* 167-178, (1963).

11. E.H. Lee and D.T. Liu, "Finite Strain Elastic-Plastic Theory Particularly for Plane Wave Analysis," *J. Appl. Phys., 38,* 19-27, (1967).

12. S. Nemat-Nasser, "Decomposition of Strain Measures and Their Rates in Finite Deformation Elastoplasticity," *Int. J. Solids Struct., 15,* 155-166 (1979).

13. J.C. Nagtegaal and J. E. DeJong, "Some Computational Aspects of Elastic-Plastic Large Strain Analysis," *Int. J. Num. Meth. Eng., 17,* 15 (1981).

14. A.E. Green and P.M. Naghdi, "Some Remarks on Elastic-Plastic Deformation at Finite Strain," *Int. J. Engng. Sci., 9,* 1219-1229 (1971).

15. T.J.R. Hughes and K.S. Pister, "Consistent Linearization in Mechanics of Solids and Structures," *Computers and Structures, 8,* 391-397 (1978).

16 W. Prager and P.G. Hodge, **Theory of Perfectly Plastic Solids,** John Wiley & Sons, 1963.

17 D.G. Ebin and J.E. Marsden, "Groups of Diffeomorphisms and the Motion of an Incompressible Fluid," *Ann. of Math., 92,* 102 (1970).

18. P.M. Pinsky, "A Numerical Formulation for the Finite Deformation Problem of Solids with Rate-Independent Constitutive Equations," *Ph.D. Dissertation*, Dept. Civil Eng., University of California, Berkeley, California, December 1981.

19. R.D. Krieg, and S. W. Key, "Implementation of a Time-Independent Plasticity Theory into Structural Computer Programs," in: J. A. Stricklin and K. J. Saczalski (Eds.), *Constitutive Equations in Viscoplasticity: Computational and Engineering Aspects*, AMD, Vol. 20, ASME, 125 (1976).

20. T.J.R. Hughes and J. Winget, "Finite Rotation Effects in Numerical Integration of Rate Constitutive Equations Arising in Large-Deformation Analysis," *Int. J. Num. Meth. Eng.*, *15*, No. 12, December 1980.

21. D. Durban and M. Baruch, "Incremental Behavior of an Elasto-Plastic Continuum," TAE Report No. 193, Dept. of Aeronautical Eng., Israel Institute of Technology, Haifa, Israel, February 1975.

22. J.E. Marsden and T.J.R. Hughes, "Topics in the Mathematical Foundations of Elasticity," in R.J. Knops (Ed.), **Nonlinear Analysis and Mechanics**, Heriot-Watt Symposium, Vol. II, Pitman Publishing Co., 1978.

23. M.E. Gurtin, **Topics in Finite Elasticity**, CBMS-NSF Regional Conference Series in Applied Mathematics, 1981.

24. C. Truesdell, "The Simplest Rate Theory of Pure Elasticity," *Comm. Pure Appl. Math.*, *8*, 123-132, 1955.

25. J.G. Oldroyd, "On the Formulation of Rheological Equations of State," *Proc. Roy. Soc.*, *A200*, 523-541, 1950.

26. B.A. Cotter and R.S. Rivlin, "Tensors Associated with Time-Dependent Stress," *Quart. Appl. Math.*, *13*, 177-182, 1955.

27. G. Jaumann, "Geschlossenes System Physikalischer und Chemischer Differentialgesetze," *Sitzungsber. Akad. Wiss. Wien (2a)*, *120*, 385-530, 1911.

28. P.M. Pinsky, M. Ortiz and K.S. Pister, "Rate Constitutive Equations in Finite Deformation Analysis: Theoretical Aspects and Numerical Integration," *Computer Methods in Applied Mechanics and Engineering*, (to appear).

29. R.D. Krieg and D.B. Krieg, "Accuracies of Numerical Solution Methods for the Elastic-Perfectly Plastic Model," *ASME J. Pressure Vessel Tech.*, **99**, 510-515, (1977).

30. H.L. Schreyer, R.F. Kulak and J.M. Kramer, "Accurate Numerical Solutions for Elastic-Plastic Models," *ASME J. Pressure Vessel Tech.*, **101**, 226-234, (1979).

31. J.M. Santiago, "On the Accuracy of Flow Rule Approximations Used in Structural and Solid Response Computer Programs," in: *Proceedings of the 1981 Army Numerical Analysis And Computers Conference*, ARO Report 81-3, (1981).

32. A. Mendelson, **Plasticity: Theory and Application,** McMillan, 1968.

33. M. Ortiz and P.M. Pinsky, "Global Analysis Methods for the Solution of the Elastoplastic and Viscoplastic Dynamic Problems," Report No. UCB/SESM-81/08, Department of Civil Engineering, University of California, Berkeley, California, December, 1981.

34. H. Brézis, *Opérateurs Maximaux Monotones et Semi-Groupes de Contractions dans les Espaces de Hilbert*, North-Holland, 1973.

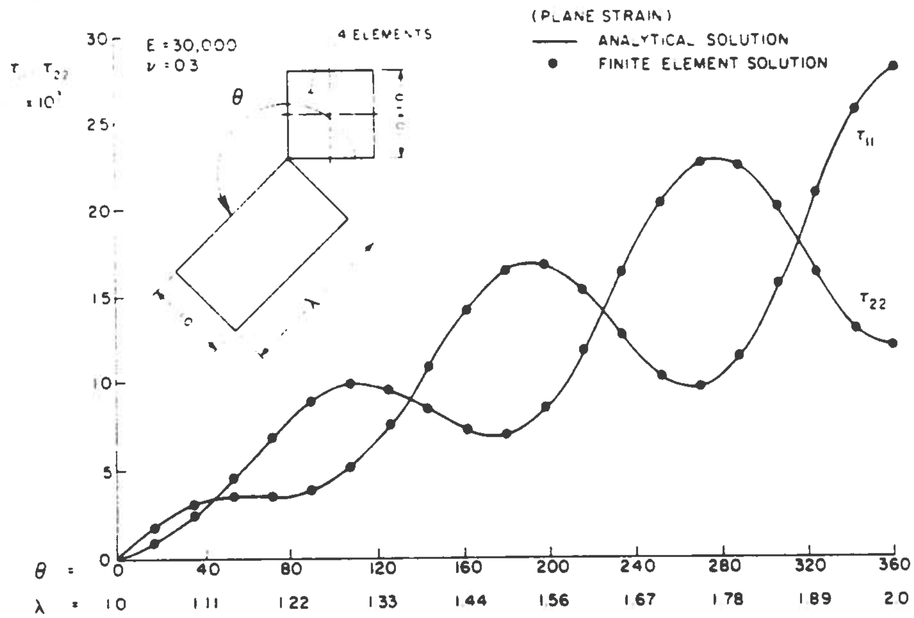

Fig. 1. Homogeneous finite simple extension and rotation. Kirchhoff stresses τ_{11} and τ_{22} versus axial stretch and rotation. Elastic constants $E = 30{,}000$, $\nu = 0.3$.

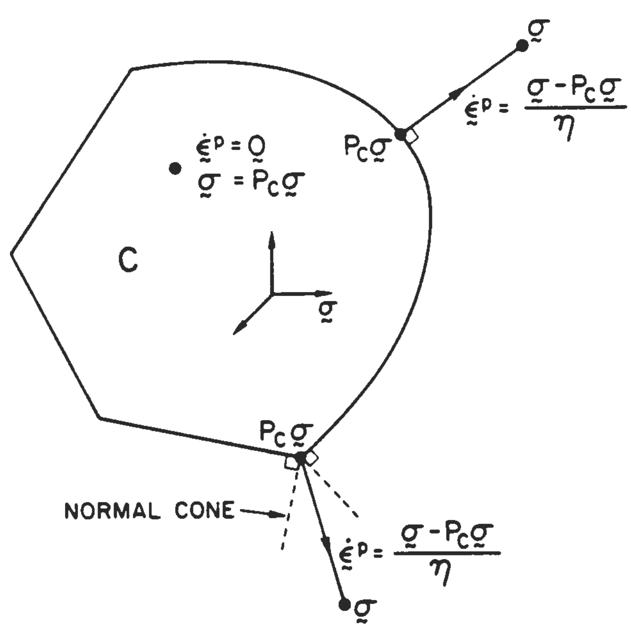

Fig. 2. Definition of viscoplastic constitutive mapping.

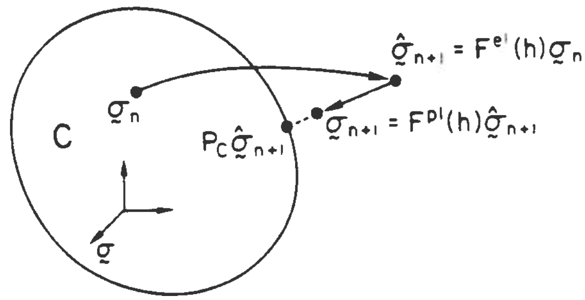

Fig. 3. Schematic representation of product algorithm.

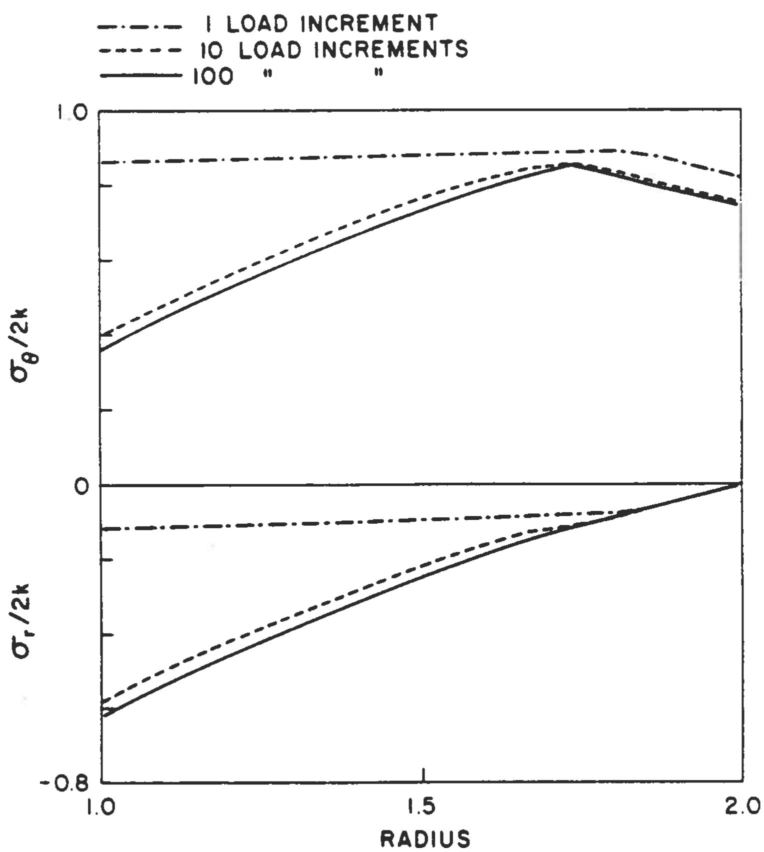

Fig. 4. Product formula solutions for an internally pressurized thick walled cylinder illustrating the rate of convergence of the algorithm. The results correspond to perfect plasticity with von Mises yield criterion and to a prescribed inner radial displacement $2Gu/ka = 1.5$, G = shear modulus, k = shear yield stress, a = inner radius.

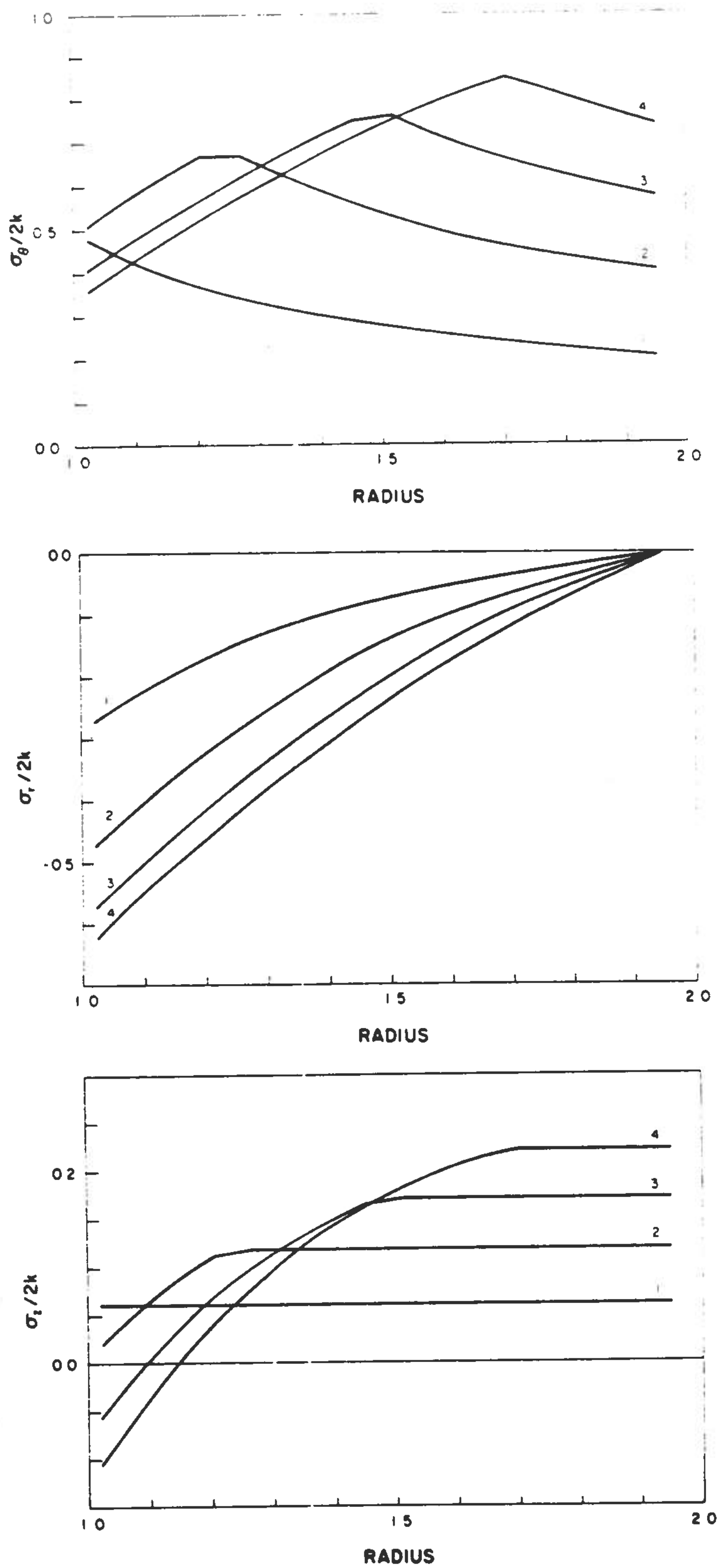

Fig. 5. Product formula solutions for an internally pressurized thick walled cylinder, with perfect plasticity and von Mises yield criterion. Curves 1-4 correspond to prescribed inner radial displacements $2Gu/ka$ = 0.5, 1.0, 1.5, 2.0, G = shear modulus, k = shear yield stress, a = inner radius, and 20 displacement increments from curve to curve.

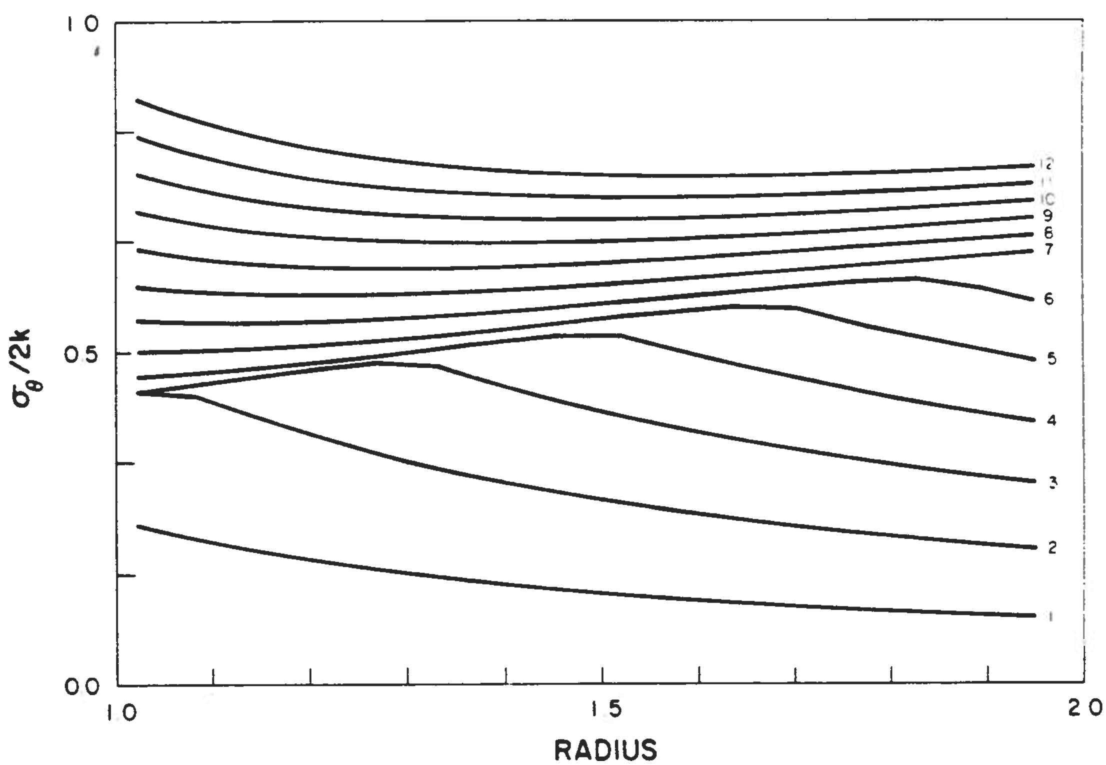

Fig. 8. Product formula solutions for an internally pressurized thick walled cylinder with isotropic hardening plasticity and von Mises yield criterion. Curves 1-12 correspond to a plastic modulus $H/E = 0.1$, $E =$ Young's modulus, prescribed inner radial displacements $3Gu/ka = 1,2,\ldots,12$, $G =$ shear modulus, $k =$ shear yield stress, $a =$ inner radius, and 2 displacement increments from curve to curve. Poisson's ratio ν was taken as 0.3.

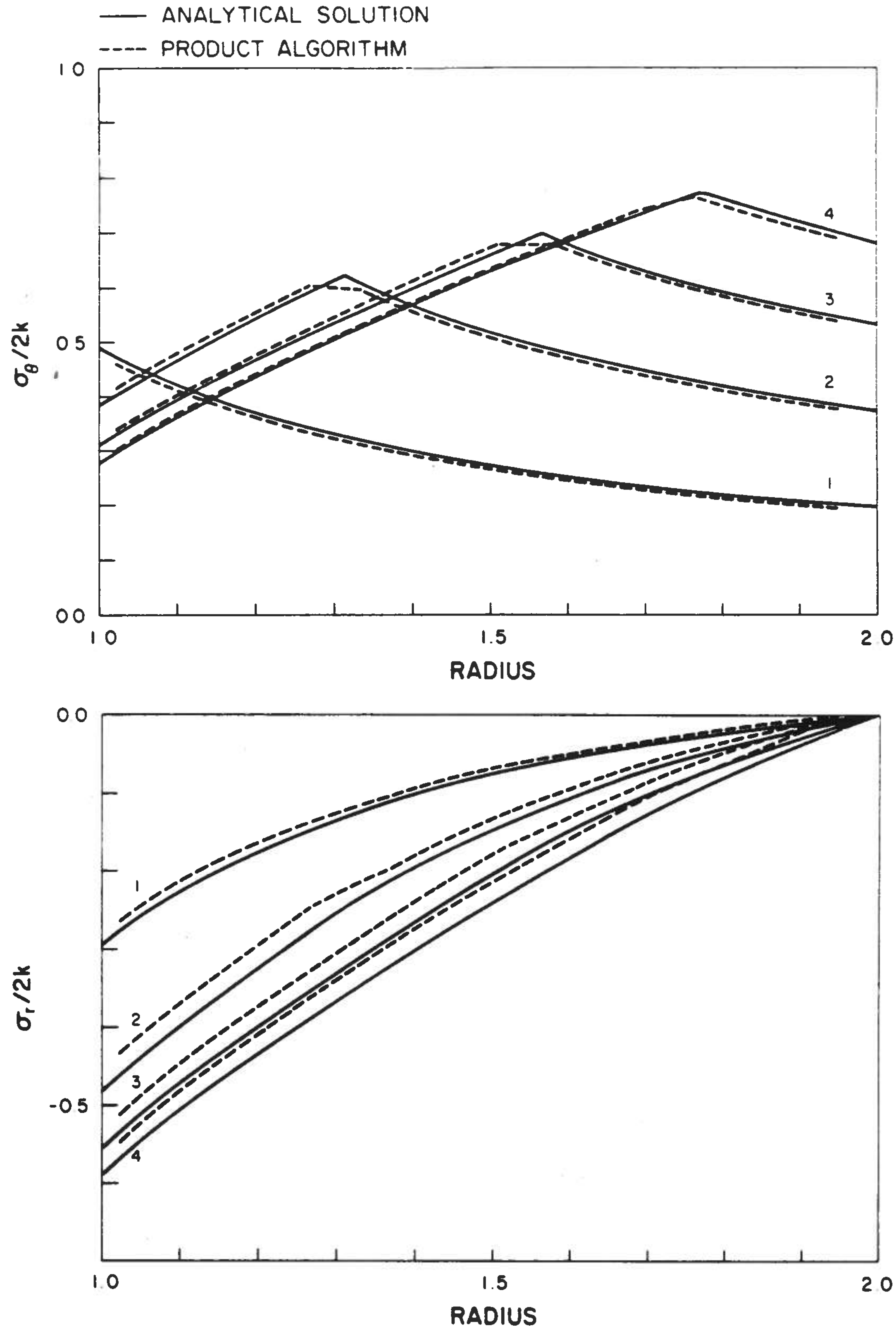

Fig. 6. Product formula solutions for an internally pressurized disk, with perfect plasticity and a Tresca yield criterion. Curves 1-4 correspond to prescribed inner radial displacements $2Gu/ka = 0.5, 1.0, 1.5, 2.0$, G = shear modulus, k = shear yield stress, a = inner radius, and 20 displacement increments from curve to curve.

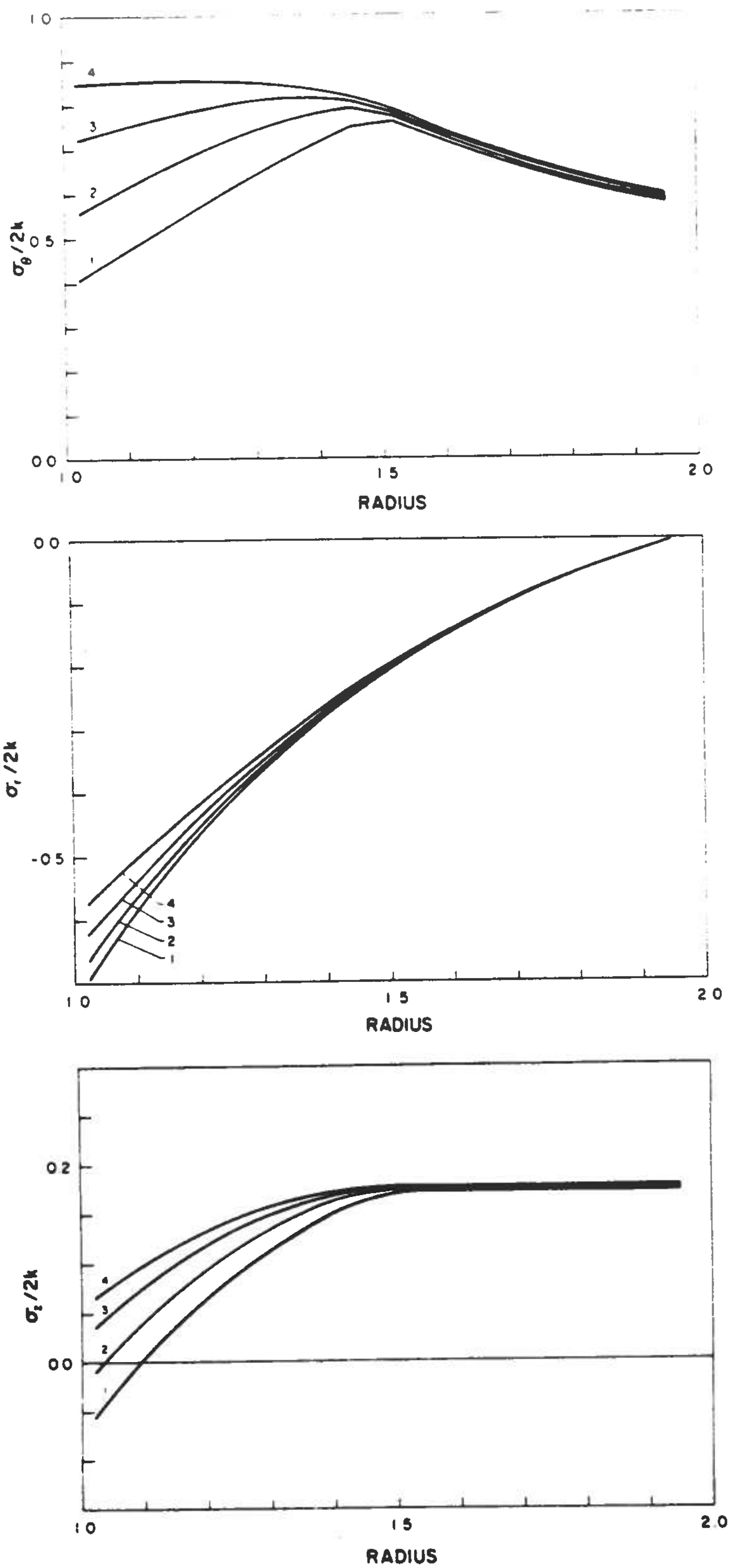

Fig. 7. Product formula solutions for an internally pressurized thick walled cylinder with perfect viscoplasticity and von Mises yield criterion. Curves 1-4 correspond to viscosities $\eta/Gh = 0, 5, 10, 15$, $G =$ shear modulus, $h =$ time step, and a prescribed inner radial displacement $2Gu/ka = 1.5$. The solution was obtained in 60 time steps.